Title	Effect of intravalley acoustic phonon scattering on quantum transport in multigate silicon nanowire metal-oxide-semiconductor field-effect transistors
Authors	Akhavan, Nima Dehdashti;Afzalian, Aryan;Lee, Chi-Woo;Yan, Ran;Ferain, Isabelle;Razavi, Pedram;Yu, Ran;Fagas, Gíorgos;Colinge, Jean-Pierre
Publication date	2010
Original Citation	Akhavan, N. D., Afzalian, A., Lee, C.-W., Yan, R., Ferain, I., Razavi, P., Yu, R., Fagas, G. and Colinge, J.-P. (2010) 'Effect of intravalley acoustic phonon scattering on quantum transport in multigate silicon nanowire metal-oxide-semiconductor field-effect transistors', Journal of Applied Physics, 108(3), 034510 (8pp). doi: 10.1063/1.3457848
Type of publication	Article (peer-reviewed)
Link to publisher's version	http://aip.scitation.org/doi/10.1063/1.3457848 - 10.1063/1.3457848
Rights	© 2010, American Institute of Physics. This article may be downloaded for personal use only. Any other use requires prior permission of the author and AIP Publishing. The following article appeared in Akhavan, N. D., Afzalian, A., Lee, C.-W., Yan, R., Ferain, I., Razavi, P., Yu, R., Fagas, G. and Colinge, J.-P. (2010) 'Effect of intravalley acoustic phonon scattering on quantum transport in multigate silicon nanowire metal-oxide-semiconductor field-effect transistors', Journal of Applied Physics, 108(3), 034510 (8pp). doi: 10.1063/1.3457848 and may be found at http://aip.scitation.org/doi/10.1063/1.3457848
Download date	2024-04-19 01:54:55
Item downloaded from	https://hdl.handle.net/10468/4744

University College Cork, Ireland
Coláiste na hOllscoile Corcaigh

Effect of intravalley acoustic phonon scattering on quantum transport in multigate silicon nanowire metal-oxide-semiconductor field-effect transistors

Nima Dehdashti Akhavan, Aryan Afzalian, Chi-Woo Lee, Ran Yan, Isabelle Ferain, Pedram Razavi, Ran Yu, Giorgos Fagas, and Jean-Pierre Colinge

Citation: Journal of Applied Physics **108**, 034510 (2010); doi: 10.1063/1.3457848
View online: http://dx.doi.org/10.1063/1.3457848
View Table of Contents: http://aip.scitation.org/toc/jap/108/3
Published by the American Institute of Physics

Effect of intravalley acoustic phonon scattering on quantum transport in multigate silicon nanowire metal-oxide-semiconductor field-effect transistors

Nima Dehdashti Akhavan,[1] Aryan Afzalian,[1,2] Chi-Woo Lee,[1] Ran Yan,[1] Isabelle Ferain,[1] Pedram Razavi,[1] Ran Yu,[1] Giorgos Fagas,[1] and Jean-Pierre Colinge[1]
[1]*Tyndall National Institute, University College Cork, Cork, Ireland*
[2]*Laboratoire de Microélectronique, Université catholique de Louvain, Louvain-la-Neuve, Belgium*

(Received 23 March 2010; accepted 31 May 2010; published online 6 August 2010)

In this paper we investigate the effects of intravalley acoustic phonon scattering on the quantum transport and on the electrical characteristics of multigate silicon nanowire metal-oxide-semiconductor field-effect transistors. We show that acoustic phonons cause a shift and broadening of the local DOS in the nanowire, which modifies the electrical characteristics of the device. The influence of scattering on off-state and on-state currents is investigated for different values of channel length. In the ballistic transport regime, source-to-drain tunneling current is predominant, whereas in the presence of acoustic phonons, diffusion becomes the dominant current transport mechanism. A three-dimensional quantum mechanical device simulator based on the nonequilibrium Green's function formalism in uncoupled-mode space has been developed to extract device parameters in the presence of electron–phonon interactions. Electron–phonon scattering is accounted for by adopting the self-consistent Born approximation and using the deformation potential theory. © *2010 American Institute of Physics*. [doi:10.1063/1.3457848]

I. INTRODUCTION

As the channel length of metal-oxide-semiconductor field-effect transistor (MOSFET) devices shrinks down to nanometer scales, short-channel effects become quite important and the control of the channel electrostatics by the gate is compromised. To help with this problem, thin-film silicon on insulator (SOI) and multigate nanowire transistor structures have been introduced.[1–3] Due to strong quantum confinement, semiclassical transport models can no longer predict the behavior of electronic transport accurately in nanowire devices. Different groups have modeled the electrical characteristics of multigate silicon nanowires in the ballistic transport regime using techniques based on the Schrödinger equation, the Wigner function, the density matrix or the nonequilibrium Green's function (NEGF) method.[4–8] The NEGF approach has been successfully used to model different types of low-dimensional structures such as carbon nanotube FETs, quantum-well devices, silicon nanowire transistors, and molecular devices.[7,9–11] The reason for the wide acceptance of the NEGF method lies in the ability it has to handle different types of elastic and inelastic scattering mechanisms such as electron–phonon and surface roughness. Different groups have investigated the effect of dissipative scattering on the electronic transport and electrical characteristics in structures such as CNTFETs and quantum-well devices.[9,12,13] There are, however, few papers discussing the effects of scattering on the electrical characteristics behavior of multigate nanowire transistors.[4,12,14–16]

Wang *et al.*[4] studied the electron–phonon interaction using the Büttiker probe technique but this phenomenological model yields only a macroscopic and semiclassical description of scattering. The Büttiker probe technique is known to sometimes predict unphysically high tunneling leakage in the off-state.[17] A rigorous treatment of scattering within the NEGF formalism and its application to multigate silicon nanowire transistors was first presented by Jin *et al.*[12] where they studied the effect of electron–phonon scattering on the low-field mobility in the long channel limit. However in their study they neither considered the self-consistent coupling of scattering self-energies and density of states (DOS) nor the current reduction mechanisms.

Here we perform a detailed study of intravalley acoustic phonon scattering (AP scattering) using the self-consistent Born approximation and its effects on the drain current and mobility of trigate FET silicon nanowire transistor. The current reduction mechanisms due to AP scattering in the subthreshold and above threshold regions will be described. Finally, it will be shown that acoustic phonons do not have any effect on the subthreshold current of short-channel nanowire transistors. The three-dimensional (3D) quantum transport equations were solved by NEGF formalism in the uncoupled mode space approach using the parabolic effective mass approximation.

II. DEVICE DESIGN AND SIMULATION

A comprehensive description of the use of the NEGF formalism and the self-consistent Born approximation to consider electron–phonon interaction can be found in the literature.[4,9,12] For clarity, however, we will give a brief overview of the technique used to build a one–dimensional (1D) mode-space Hamiltonian from a 3D real-space Hamiltonian and how to consider AP scattering in the equations. The idea behind mode-space NEGF simulations is to decouple the 3D wave function into an energy variation in the ID-transport direction and two-dimensional (2D) wave function in the confinement directions. Then the 2D Schrödinger equation is

solved in each cross section to obtain the corresponding eigenvalues and eigenvectors. Having found the eigenvalues (modes) in each cross section, we apply the ID NEGF quantum transport to each mode. Assuming the x-direction as the transport direction, the 3D Schrödinger equation in a single valley can be written as:[4,18]

$$H_{3D}\Psi(x,y,z) = E\Psi(x,y,z), \tag{1}$$

where ψ is the 3D wave function and H_{3D} is the 3D device Hamiltonian. Assuming parabolic bands, the effective mass Hamiltonian becomes:

$$H_{3D} = -\frac{\hbar^2}{2}\frac{\partial}{\partial x}\left(\frac{1}{m_x^*}\frac{\partial}{\partial x}\right) - \frac{\hbar^2}{2}\frac{\partial}{\partial y}\left(\frac{1}{m_y^*}\frac{\partial}{\partial y}\right) - \frac{\hbar^2}{2}\frac{\partial}{\partial z}\left(\frac{1}{m_z^*}\frac{\partial}{\partial z}\right) + U(x,y,z). \tag{2}$$

Here, U is the self-consistent electrostatic potential energy and m_x^*, m_y^*, m_z^*, are the effective masses in the x,y,z direction of the nanowire, respectively.[7] In order to be able to solve the problem in a computation-efficient manner we adopt the mode-space approach. The ID Schrödinger in the transport direction for each mode can be written as:[4,12,19]

$$-\frac{\hbar^2}{2}\bar{a}_{mm}(x)\frac{\partial^2}{\partial x^2}\varphi^m(x) - \sum_n E_C^{mm}\varphi^m(x) + E_{sub}^m \cdot \varphi^m(x) = E\varphi^m(x), \tag{3}$$

where

$$\bar{a}_{mm}(x) = \oint_{y,z}\frac{1}{m_x^*}|\xi^m(y,z;x)|^2 dydz, \tag{4}$$

is the inverse of the average value of the effective mass in the cross section. The second term in Eq. (3) presents the coupling between modes m and n. It has been shown that if the device structure is uniform along the transport direction the mode-coupling coefficient is approximately zero and can be neglected.[12,19] In the MS approach, the energy levels and the wave function at position x along the nanowire is obtained by solving the 2D transversal Schrödinger equation in each cross section of the nanowire as follows:

$$\left[-\frac{\hbar^2}{2}\frac{\partial}{\partial y}\left(\frac{1}{m_y^*}\frac{\partial}{\partial y}\right) - \frac{\hbar^2}{2}\frac{\partial}{\partial z}\left(\frac{1}{m_z^*}\frac{\partial}{\partial z}\right) + U(y,z,x_i)\right]\xi^n(y,z;x_i) = E_{sub}^n(x_i)\xi^n(y,z,x_i), \tag{5}$$

where E_{sub} and ξ are the nth eigenvalue and wave function at position $x=x_i$ in the transport direction. From the mode-space device Hamiltonian, the retarded Green's function, G^r, of the active device can be built. Then all the internal and observable device characteristics such as local DOS, electron density and current can be extracted by solving the equations of motion for the Green's functions.[4,9,12,18]

A. The NEGF

Now that we have built the ID mode-space Hamiltonian, all other parameters including observable physical quantities can be obtained by NEGF approach. In the NEGF formalism the steady state equations of motion are written as:[12,18]

$$G^{r,a}(E) = [EI - H_{1D} - \Sigma_1 - \Sigma_2 - \Sigma_S]^{-1}, \tag{6}$$

$$G^{\langle,\rangle}(E) = G^r(E)\Sigma^{\langle,\rangle}(E)G^a(E), \tag{7}$$

where $G^{r,a}$ are retarded and advanced Green's function, $G^{\langle,\rangle}$ are lesser and greater Green's function, and $\Sigma_1(\Sigma_2)$ is the self-energy caused by the coupling between the device and the source (drain) reservoir. Σ_s is the self-energy due to electron–phonon interaction. The derivation of source and drain self-energies can be found in.[4,12] Phonon scattering consists of elastic and inelastic mechanisms, however, we only consider elastic intravalley AP scattering and neglect other types of scattering. Assuming that electron–phonon interactions are local in space, in scattering and out-scattering self-energies for inelastic electron–phonon interaction can be written as:[12,15]

$$\Sigma_v^{<,n}(x,E) = |M_q|^2 \cdot \sum_m G_v^{<,m}(x,E) \cdot I_{m,v}^{n,v}(x), \tag{8}$$

$$\Sigma_v^{>,n}(x,E) = |M_q|^2 \cdot \sum_m G_v^{>,m}(x,E) \cdot I_{m,v}^{n,v}(x), \tag{9}$$

where v is the valley index, n is the subband number, $G^{<,m}$ is the lesser Green's function of mth mode, $|M_q|^2$ the electron–phonon matrix element adopted from[12,20] and is defined as:

$$|M_q|^2 = \frac{\Xi^2 k_B T}{\rho u_l^2}, \tag{10}$$

where $\Xi(14.6\ \text{eV})$ is the acoustic phonon deformation potential, $\rho(2.329\ \text{g/cm}^3)$ is the density of silicon, and $u_l(9.05\times10^5\ \text{cm/s})$ is the velocity of sound. Finally, I represents the electron–phonon wave function overlap and is defined as:[12,21]

$$I_{m,v}^{n,v'}(x) = \oint |\xi_{x,v}^{n,v'}(y,z)|^2 \cdot |\xi_{x,v}^{m,v'}(y,z)|^2 dxdy, \tag{11}$$

where ξ is the wave function of mode n at the transverse plane in position x of transport direction. The imaginary and real part of scattering self-energy can be written as:

$$\Sigma_S^i(x,E) = -\frac{i}{2}[\Sigma_S^>(x,E) + \Sigma_S^<(x,E)], \tag{12}$$

$$\Sigma_S^r(x,E) = P\int \frac{dE'}{2\pi}\frac{\Gamma_S(x,E')}{E-E'}, \tag{13}$$

$$\Gamma_S(E) = i[\Sigma_S^>(E) - \Sigma_S^<(E)], \tag{14}$$

where Γ_S is the broadening function. The real part of self-energy is responsible for the renormalization of energies and manifests itself as an energy level shift. It has been shown that the integral in Eq. (13) does not have any significant effect on the results and can be neglected.[9,11] In the above definition of scattering self-energy, we can identify a self-consistent loop between Eqs. (7) and (12) which is performed for all the energy points. After all Green's functions have reached convergence, and after having computed the

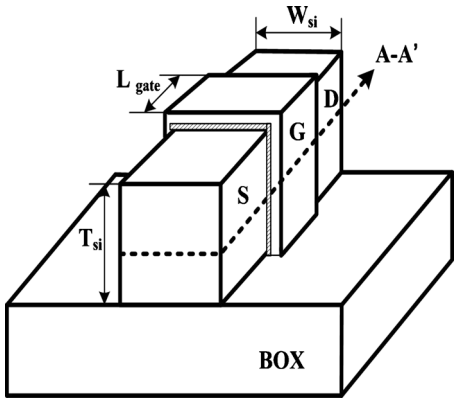

FIG. 1. Schematic view of a trigate nanowire FET with S/D extension length of 10 nm, $T_{ox}=1$ nm and a box thickness of 4 nm.

scattering self-energies, the current density flowing between layer x_i and x_{i+1} in the transport direction for each valley can be computed as follows:

$$I^{v}_{x\to x+1}=\frac{q}{h}\int_{-\infty}^{+\infty}[H_{x,x+1}G^{<,v}_{x+1,x}(E)-H_{x,x+1}G^{<,v}_{x,x+1}(E)]\frac{dE}{2\pi}, \tag{15}$$

this current should be constant for all x positions to ensure current continuity principle. The criterion has been used as convergence index for outer loop along with charge convergence.

III. RESULTS AND DISCUSSION

An overview of quantum transport in 3D nanowire including dissipative transport was presented in Sec. II. Now we discuss the effect of elastic AP electron–phonon scattering on electron transport and electrical characteristics. Here, we consider a trigate silicon nanowire FET transistor with ⟨100⟩ channel direction as presented in Fig. 1 The cross section is 5×5 nm^2. The length of the gate and the length of the source/drain (S/D) extensions is 10 nm. The buried oxide thickness is 5 nm and the back gate is grounded. The source and drain contacts are heavily doped N-type with $N_d=10^{20}$ cm^{-3} while the channel region is undoped.

In Fig. 2(a) the I_{DS}-V_{GS} curves are plotted for $V_{DS}=0.05$ V and $V_{DS}=0.4$ V and a gate length of 10 nm. It can be observed that AP scattering is the dominant scattering mechanism above threshold for short gate lengths. In Fig. 2(b) the I_{DS}-V_{GS} curves are plotted for two gate lengths using either ballistic or scattering transport. For a device with $L_g=10$ nm the currents calculated with both ballistic and dissipative transport are identical in the subthreshold region. There is, however, a slight reduction in current above threshold due to AP scattering. Thus ballistic transport is predominant below threshold and dissipative transport is more significant above threshold. For a device with $L_g=30$ nm the current in presence of AP scattering is always lower than that with ballistic transport, which means that AP scattering is present for all regimes of operation.

In order to study the mechanisms involved in current reduction by acoustic phonons, we have plotted several internal device quantities operating in either below or above

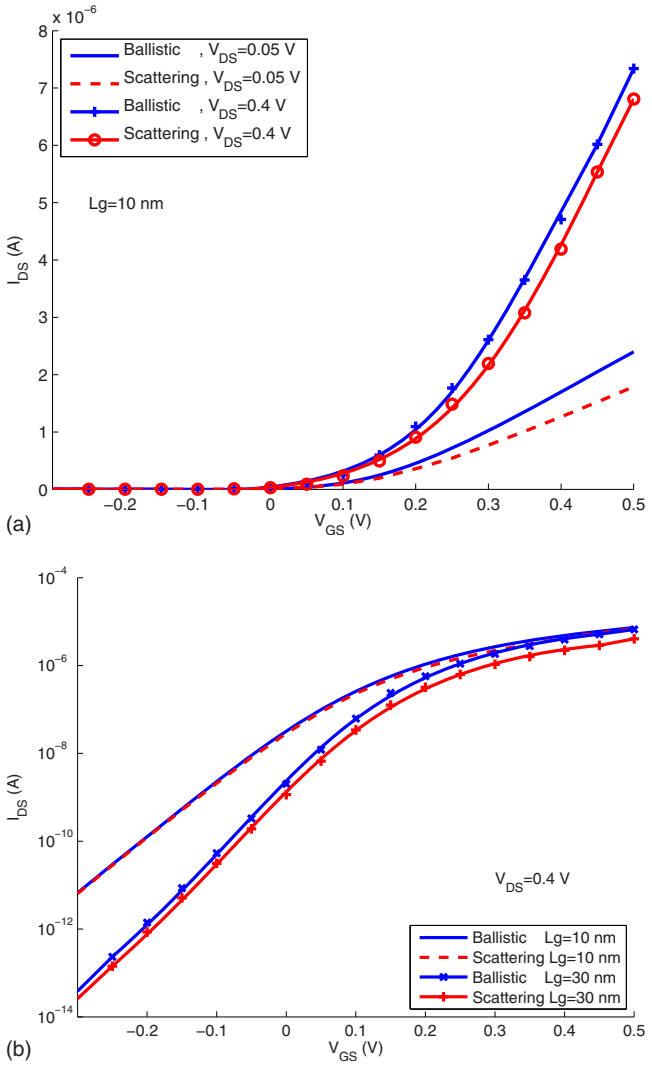

FIG. 2. (Color online) I_{DS}-V_{GS} curve at $V_{DS}=0.05$ V and $V_{DS}=0.4$ V under ballistic and dissipative transport. (a) For short-channel device ($L_g=10$ nm) we can be observed that AP scattering reduces the current above threshold and (b) in the long channel device, acoustic phonons are always dominant while for the short-channel device they are important only above threshold.

threshold. First we discuss the effect of AP scattering in nanowire with $L_g=30$ nm and $V_{DS}=0.05$ V. In Fig. 3(a) shows the energy-position-resolved current density in the subthreshold region (off-state) under ballistic and AP scattering transport. One can see that in ballistic case the drain current is dominated by tunneling through the barrier, whereas in the dissipative (scattering) transport current is been shifted to higher energies above the first subband and the main current is diffusion current. Figure 3(b) shows the energy-resolved current density above threshold. In the ballistic case, discrete resonances can be identified in the current energy spectrum due to ballistic transport at specific energy levels corresponding to position of subbands. In the presence of AP scattering, on the other hand, the spectrum is smeared across a range of energy levels due to scattering of electron by acoustic phonons. Scattering causes the electron distribution to spread over a wider range of energy levels such that a continuous current spectrum in obtained in the energy space.

Figure 4 shows the current spectrum at source and drain

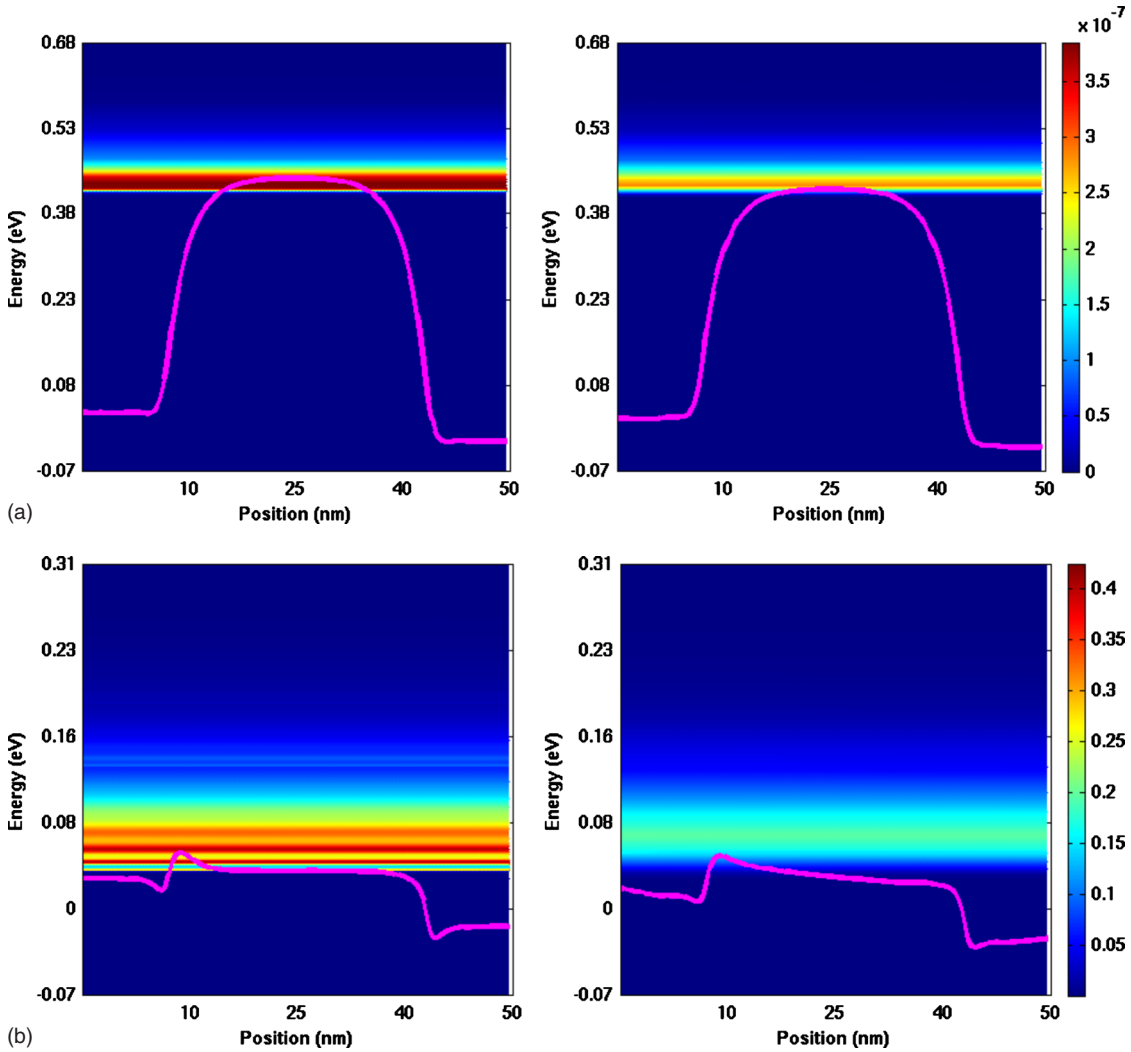

FIG. 3. (Color online) Energy-resolved current density at V_{DS}=0.05 V for L_g=30 nm (a) in off-state it can be observed that the tunneling current through the barrier is dominant in ballistic transport (left) and in the case of AP scattering (right) which shifts the current spectrum to higher energies and the diffusive current becomes dominant and (b) in the on-state both tunneling and diffusive currents take part in the case of ballistic transport (left) and resonances can be identified in the current spectrum due to participation of different subbands. AP scattering (right) smoothes the LDOS and shifts the current spectrum to higher energies above the barrier.

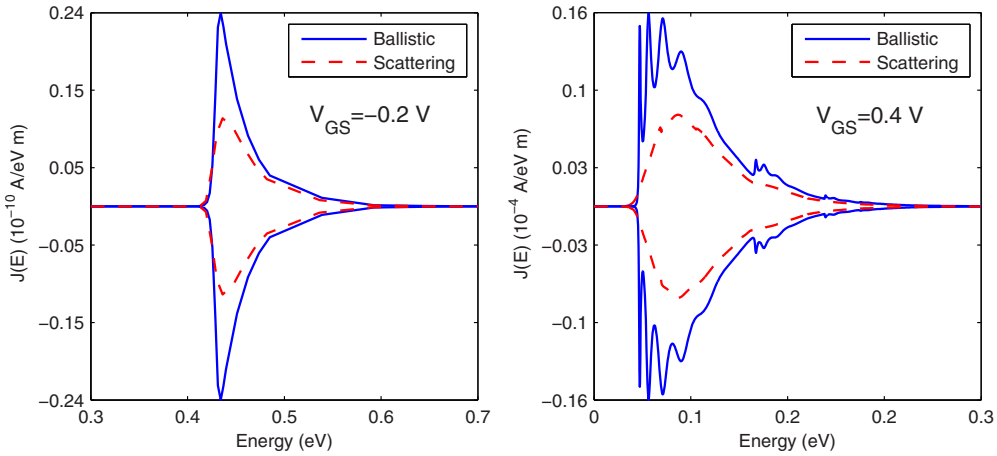

FIG. 4. (Color online) Spectrum of source (drain) current vs energy at off-state (left) and on-state (right). The source-injected current is taken as positive and the drain-collected current is taken as negative. In the ballistic case (solid line) the current spectra due to the source and drain are symmetrical because the ballistic transport does not change or modify the momentum of the electrons. In the case of AP scattering (dashed line) the source and drain currents are still symmetrical because AP scattering does not modify the energy of the electrons. The amplitude of the current has decreased compare to the ballistic case because scattered electrons change direction and are back scattered as a result of scattering.

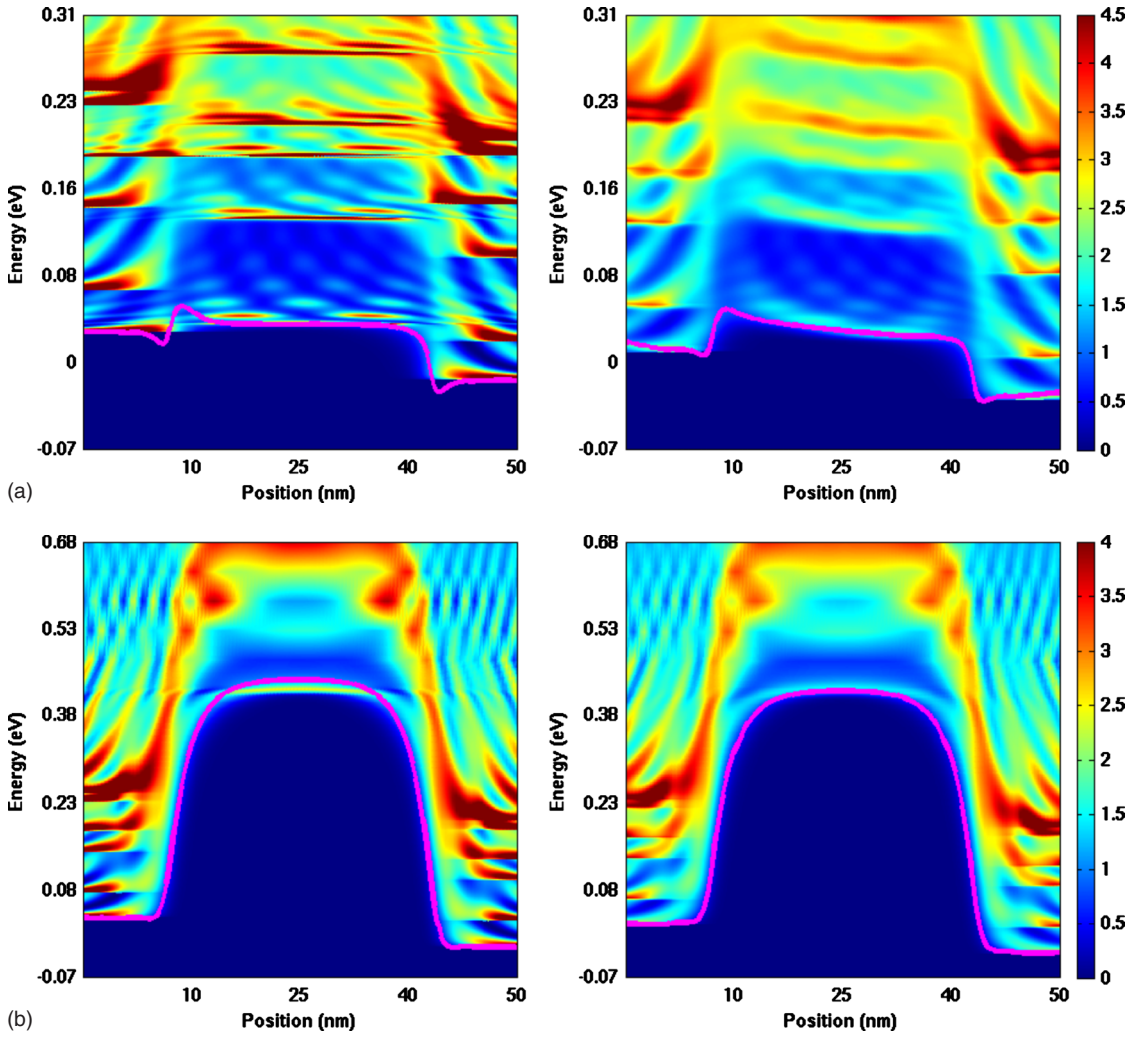

FIG. 5. (Color online) Energy-resolved LDOS (a) for L_g=30 nm and V_{DS}=0.05 V, in the off-state. It can be observed that permitted energy states are available under the barrier ballistic transport (left) whereas the LDOS is shifted above the barrier and broadened due to scattering (right) and (b) for L_g =30 nm in the on-state, it can be observed that the ballistic case creates LDOS oscillations above the barrier while transport with scattering LDOS yields a continuous LDOS spectrum.

current versus energy. In the ballistic transport regime (solid lines), electrons enter the device at the source end and leave at the drain end. We take the source-injected current as positive for electrons entering the device. Conversely, the drain-collected current is negative for electrons leaving the device. The contributions from different subbands appear as peaks in the plot. These can be clearly observed in the on-state where a maximum number of subbands participate to current transport (right). In the presence of AP scattering which is a phase breaking scatterings mechanism (i.e., electrons may change moving direction when scattered but will retain their longitudinal energy), the source and drain current spectra remain identical in shape and opposite in sign. However, the current magnitude decreases compared to the ballistic case because scattered electrons lose momentum as a result of scattering.[13,17]

To get a better understanding of the contributions of tunneling and diffusion to the current spectrum, we have plotted the LDOS of the channel region. Figure 5(a) clearly shows that there is some available DOS under the barrier in the case of ballistic transport, which causes tunneling current, the dominant transport mechanism in subthreshold operation. In the presence of scattering, the LDOS is broadened and shifted to higher energies above the first subband, which means that diffusion current is now the dominant transport mechanism. In a similar way, Fig. 5(b) represents the LDOS above threshold (on-state). One can observe that the LDOS for ballistic transport exhibits strong oscillations which are due to quantum interference whereas in the case of AP scattering LDOS has been broaden to adjacent energy levels because scattering inside the nanowire randomizes the phase of the electrons and hence destroys the quantum coherence in the device.[12,17,22]

In Fig. 6 we have plotted the energy-resolved electron density for L_g=30 nm and V_{DS}=0.4 V. In the presence of elastic AP scattering, the carriers will change direction in the channel without losing energy which leads to increase in carrier back scattering and charge reduction in channel. Moreover, the slope of the subbands in the S/D extension regions reflects the presence of S/D series resistances in the on-state. This resistance is caused by AP scattering in the heavily doped S/D regions.

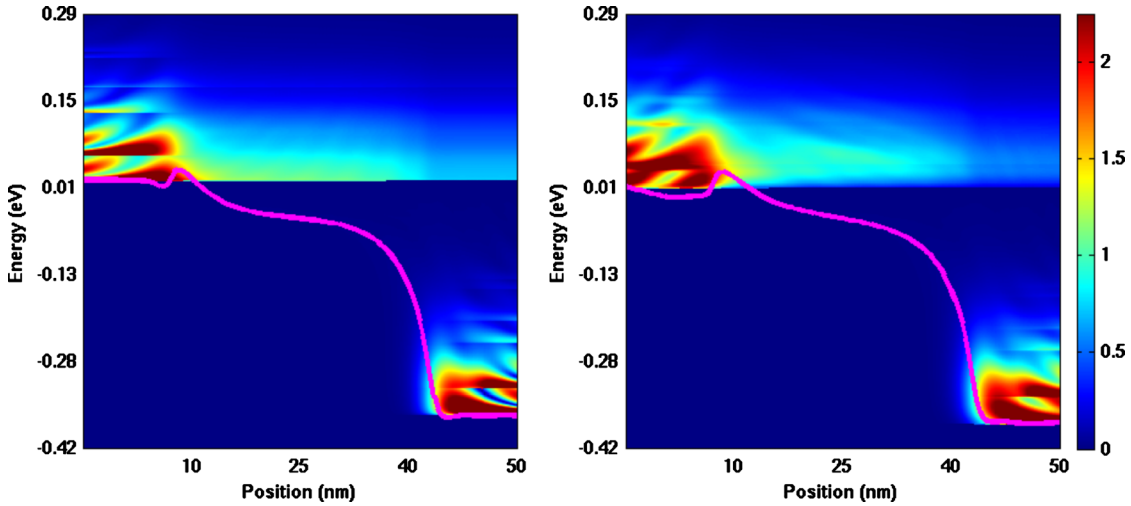

FIG. 6. (Color online) Energy-resolved electron density for L_g=30 nm, V_{DS}=0.4 V in the on-state. It can be observed that the electron density is higher in the channel for ballistic transport (left), while it has been reduced in dissipative transport due to back scattering of carriers by elastic acoustic phonons (right).

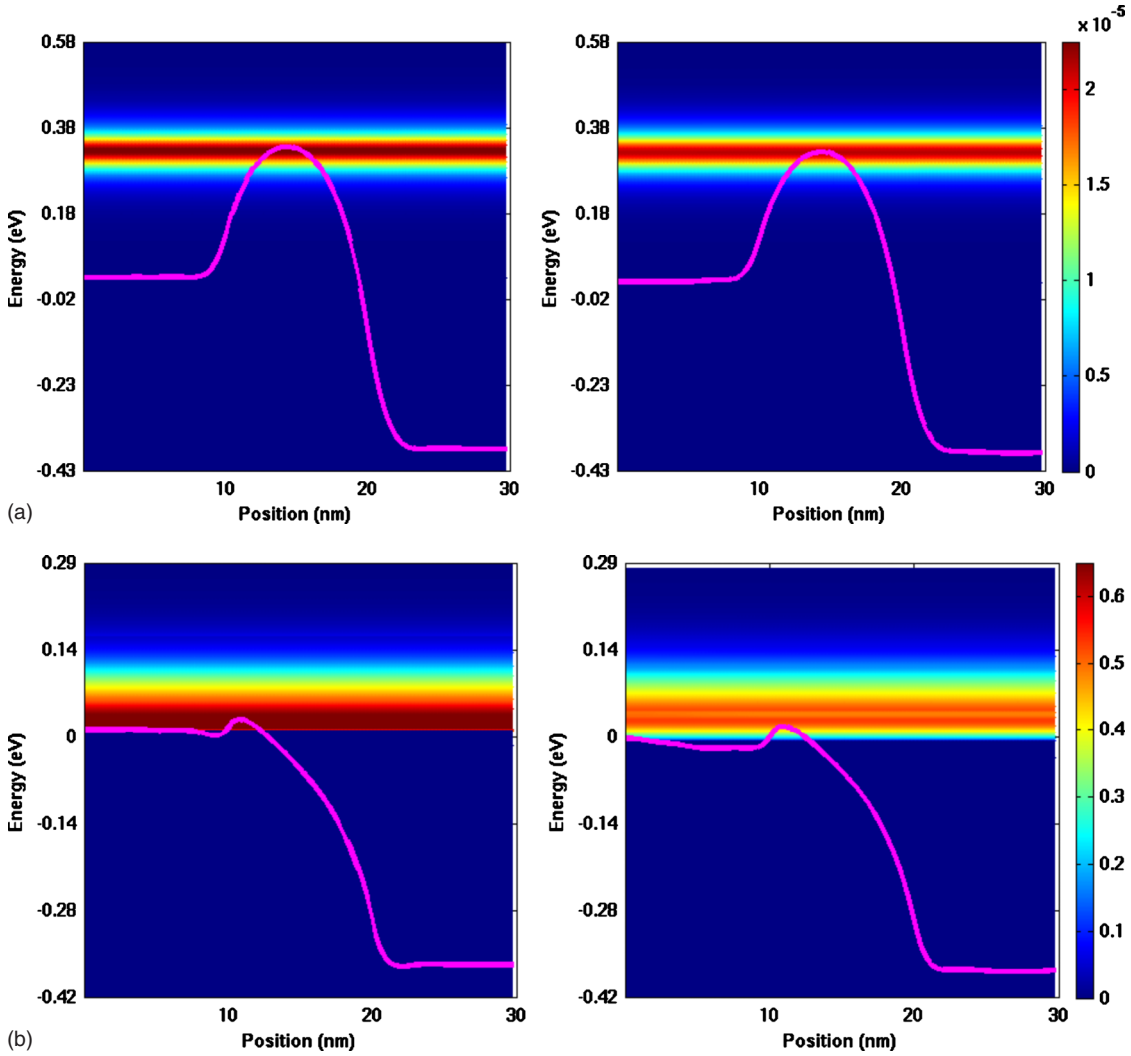

FIG. 7. (Color online) Energy-resolved current density at V_{DS}=0.4 V for L_g=10 nm in both on-state and off-state. The current has following two parts: a diffusive component above the barrier with resonances and a tunneling component part through barrier, (a) in the off-state there is no major difference between ballistic and AP scattering and (b) in the on-state the diffusive current is dominant as scattering has shifted the current spectrum to higher energies.

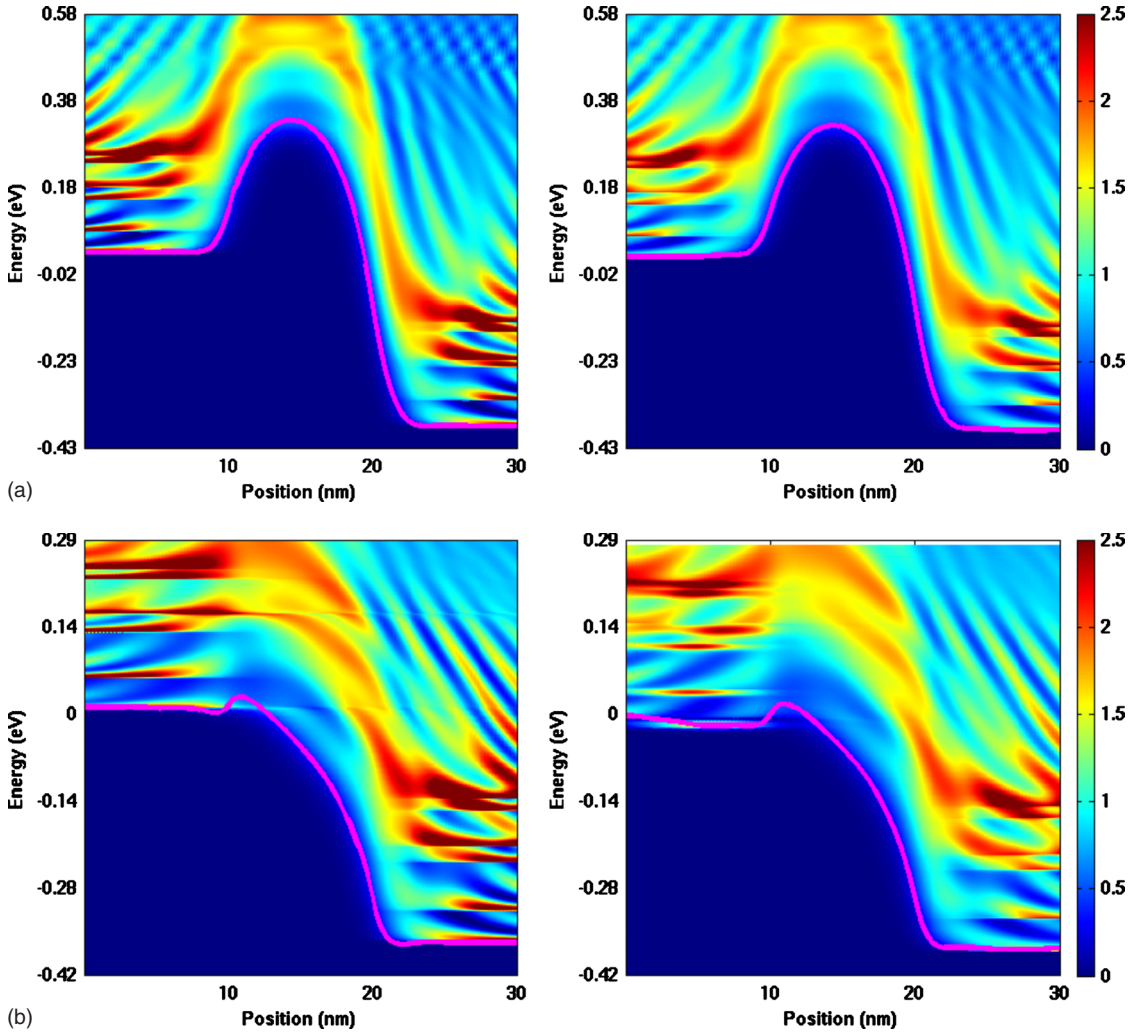

FIG. 8. (Color online) Energy-resolved LDOS for L_g=10 nm and V_{DS}=0.4 V (a) it can be observed that the LDOS retains the oscillatory shape under ballistic and dissipative transport in the off-state and (b) in the on-state, LDOS is available under the barrier due to ballistic transport. It is shifted to the top of the barrier and broadened due to AP scattering in dissipative transport.

Now we discuss the characteristics of short-channel device with L_g=10 nm and V_{DS}=0.4 V in subthreshold (off-state) and above threshold (on-state). Figure 7(a) shows that in the off-state both tunneling and diffusion current are contributing to the total current of ballistic and dissipative transport, respectively. In the on-state, the tunneling current through the potential barrier remains the dominant current in the case of purely ballistic transport while the diffusion current becomes dominant in the case of dissipative transport. Similarly, Fig. 8 shows the LDOS at on-state and off-state of nanowire with L_g=10 nm. Here, unlike the long channel device there is no distinct LDOS under the barrier because of the small barrier height, there is relatively strong tunneling current in the case of ballistic transport at on-state while, the tunneling current disappears in the case of dissipative transport.

The $I_{on}(I_{off})$ current dependence on gate length and silicon thickness has also been studied. Figure 9 shows the $I_{\text{phonon}}/I_{\text{ballistic}}$ ratio as a function of L_g, where $I_{\text{phonon}}(I_{\text{balliostic}})$ is the drain current at on-state for ballistic and scattering case and is defined as:

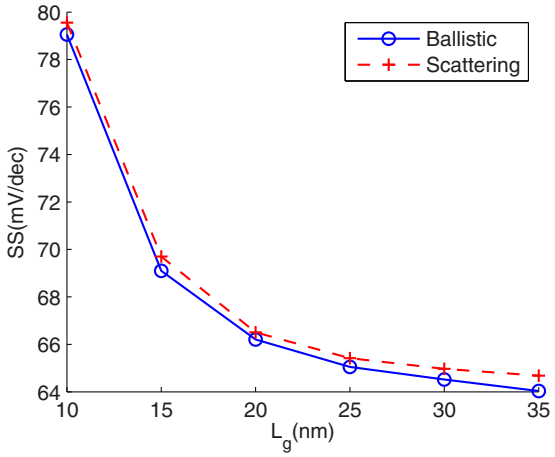

FIG. 9. (Color online) Degree of ballisticity in nanowire transistors for different values of silicon thickness and gate lengths, as a function of I_{on} and I_{off}, respectively. AP scattering become less important as gate length is decreased due to reduction in electron density which determines the electron–phonon interaction strength.

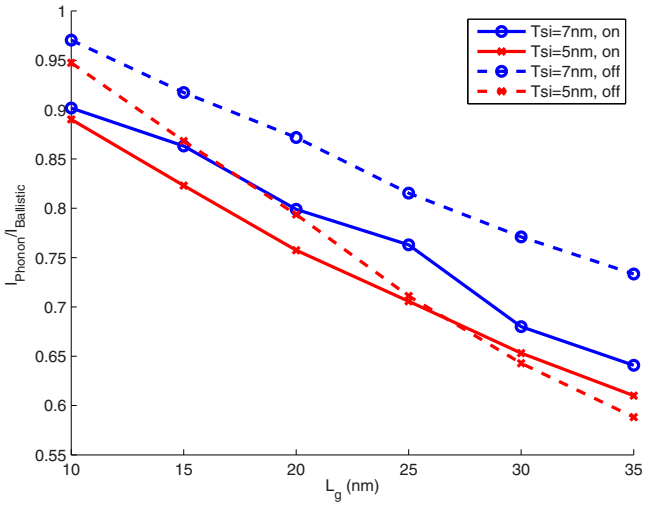

FIG. 10. (Color online) SS as a function of gate length. Due to higher impact of AP above threshold, SS has become worse in dissipative transport. However, as we decrease the gate length it gets closer to the ballistic limit.

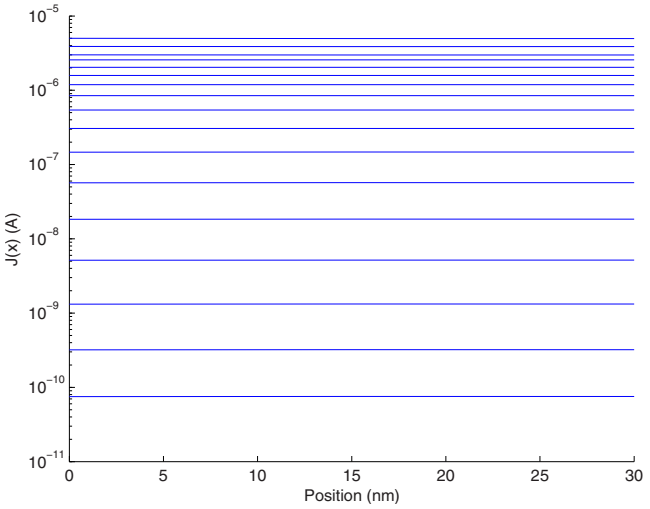

FIG. 11. (Color online) Plot of current continuity along the channel for different values of V_{GS} at V_{DS}=0.4 V and L_g=30 nm. It can be observed that the current has been conserved in the presence of scattering at all slices in the transport direction.

$$I_{ON} = I_{DS}(V_{GS} - V_T = 0.4 \text{ V}, V_{DS} = 0.4 \text{ V}), \tag{16}$$

where V_T is the threshold voltage. The ballisticity curves show that AP scattering become less important as the gate length is decreased. The reason for this effect is that the electron density which determines the electron–phonon interaction strength and contributes to back scattering of carriers is directly proportional to the gate length of the device. Figure 10 shows the variation in subthreshold swing (SS) versus gate length for ballistic and scattering mechanisms. Due to higher impact of electron–phonon interaction on on-current we observe a slight reduction in SS. However, as we reduce the gate length the difference in SS becomes negligible due to reduction in probability for electrons to be back scattered.[16,23]

Throughout all simulations we always check the continuity of the current (15) at all points along the transport direction as additional convergence criterion to charge to ensure the correctness of obtained results. This has been presented in Fig. 11 for V_{DS}=0.4 V and $0 < V_{GS} < 0.6$ where error of 1% has been used as a limit for total current change at each point x_i along the device.

IV. CONCLUSION

We investigated the effect of intravalley AP scattering on quantum transport in multigate silicon nanowire FETs. We find out that phonon scattering strongly decreases ballistic tunneling through the barrier and transforms the dominant drain current from tunneling to diffusion current above the barrier. AP scattering also causes broadening of the LDOS in the nanowire due to randomization of electron momentum in the transport direction. We also presented the degree of ballisticity in nanowire transistors with respect to gate length and thickness.

ACKNOWLEDGMENTS

This work is supported by the Science Foundation Ireland Grant No. 05/IN/I888: Advanced Scalable Silicon-on-Insulator Devices for Beyond-End-of-Roadmap Semiconductors. This work has also been enabled by the Programme for Research in Third-Level Institutions. This work was supported in part by the European Community (EC) Seventh Framework Program through the Networks of Excellence NANOSIL and EUROSOI+ under Contract Nos. 216171 and 216373.

[1] M. Shin, IEEE Trans. Nanotechnol. **6**, 230 (2007).
[2] J. P. Colinge, Solid-State Electron. **51**, 1153 (2007).
[3] J. P. Colinge, *Nanoscaled Semiconductor-on-Insulator Structures and Devices*, NATO Science for Peace and Security Series B: Physics and Biophysics, pp. 159–164, 2007).
[4] J. Wang, E. Polizzi, and M. Lundstrom, J. Appl. Phys. **96**, 2192 (2004).
[5] Y. Yamada, H. Tsuchiya, and M. Ogawa, IEEE Trans. Electron Devices **56**, 1396 (2009).
[6] S. Barraud, J. Appl. Phys. **106**, 063714 (2009).
[7] A. Martinez, M. Bescond, J. R. Barker, A. Svizhenko, M. P. Anantram, C. Millar, and A. Asenov, IEEE Trans. Electron Devices **54**, 2213 (2007).
[8] A. R. Brown, A. Martinez, N. Seoane, and A. Asenov, *Comparison of Density Gradient and NEGF for 3D Simulation of a Nanowire MOSFET*, Proceedings of the Spanish Conference on Electron Devices (CDE), Feb. 11–13, Santiago de Compostela, Spain, pp. 140–143, 2009.
[9] S. O. Koswatta, S. Hasan, M. S. Lundstrom, M. P. Anantram, and D. E. Nikonov, IEEE Trans. Electron Devices **54**, 2339 (2007).
[10] M. Pourfath, H. Kosina, and S. Selberherr, J. Phys.: Conf. Ser. **109**, 012029 (2008).
[11] M. Pourfath, H. Kosina, and S. Selberherr, Math. Comput. Simul. **79**, 1051 (2008).
[12] S. Jin, Y. J. Park, and H. S. Min, J. Appl. Phys. **99**, 123719 (2006).
[13] M. Pourfath, H. Kosina, and S. Selberherr, J. Phys.: Conf. Ser. **38**, 29 (2006).
[14] M. Luisier and G. Klimeck, Phys. Rev. B **80**, 155430 (2009).
[15] K. Rogdakis, S. Poli, E. Bano, K. Zekentes, and M. G. Pala, Nanotechnology **20**, 295202 (2009).
[16] S. Poli and M. G. Pala, IEEE Electron Device Lett. **30**, 1212 (2009).
[17] R. Venugopal, M. Paulsson, S. Goasguen, S. Datta, and M. S. Lundstrom, J. Appl. Phys. **93**, 5613 (2003).
[18] N. D. Akhavan, A. Afzalian, C. W. Lee, R. Yan, I. Ferain, P. Razavi, G. Fagas, and J. P. Colinge, IEEE Trans. Electron Devices **57**, 1102 (2010).
[19] A. Afzalian, N. D. Akhavan, and C. W. Lee, Y. R. I. Ferain, P. Razavi, and J. P. Colinge, J. Comput. Electron. **8**, 287 (2009).
[20] A. Svizhenko and M. P. Anantram, IEEE Trans. Electron Devices **50**, 1459 (2003).
[21] E. B. Ramayya, D. Vasileska, S. M. Goodnick, and I. Knezevic, J. Appl. Phys. **104**, 063711 (2008).
[22] J. Guo, J. Appl. Phys. **98**, 063519 (2005).
[23] H. Tsuchiya and S. Takagi, IEEE Trans. Electron Devices **55**, 2397 (2008).